Journal of Earthquake and Tsunami

Evolution of Elastic Shear Modulus During Shearing Under Different Stress Paths Considering Anisotropic Stress History

--Manuscript Draft--

Manuscript Number:	WSPC-JET-D-23-00089R2
Full Title:	Evolution of Elastic Shear Modulus During Shearing Under Different Stress Paths Considering Anisotropic Stress History
Article Type:	Research Paper
Keywords:	Shear Modulus, Stress Path, Anisotropic Consolidation, Stress History
Corresponding Author:	Ali Akhtarpour Ferdowsi University of Mashhad Faculty of Engineering IRAN (ISLAMIC REPUBLIC OF)
Corresponding Author Secondary Information:	
Corresponding Author's Institution:	Ferdowsi University of Mashhad Faculty of Engineering
Corresponding Author's Secondary Institution:	
First Author:	Kamran Fani
First Author Secondary Information:	
Order of Authors:	Kamran Fani
	Ali Akhtarpour
	Jafar Bolouri Bazaz
Order of Authors Secondary Information:	
Abstract:	Continuous shear wave velocity measurements are conducted on cylindrical triaxial sandy specimens consolidated with isotropic and anisotropic stress histories to characterize the evolution of the elastic shear modulus under different stress paths. The shear wave velocity is measured using an automatic device capable of consecutive measurements of travel time. All specimens were prepared using the Water Sedimentation (WS) method, and after undergoing a stress-controlled path representing the stress history of the specimens, they were subjected to stress-controlled drained shearing along eight different paths. The stress components used in the existing correlations estimating the shear moduli are specified under different stress paths. The results demonstrate that the existing empirical correlations can appropriately be used within the elastic region or the loading surface. However, the accuracy of such models estimating shear moduli might be depreciated as shearing commences, particularly if the stress path involves deviatoric stress, diverging from the expected trends at a specific stress ratio, which is strongly linked to the consolidation stress state. A criterion at which the shear modulus is diverted is also suggested, found to be directly related to the initial stress anisotropy.
Response to Reviewers:	Reviewer #1: C0: Reviewer #1: The manuscript may be accepted for publication as is. R0: Thanks indeed for the time and attention dedicated to this manuscript, without hesitation, enriching the quality of the manuscript. Reviewer #2: Co: The revised manuscript has been significantly improved. However, my main concern goes to the manuscript's subject, which falls outside the main keywords of the journal. Instead, it is more suitable for a specialized geotechnical engineering journal. To somehow resolve this issue, the authors are recommended to consider the following comments:

R0: Thanks indeed for the time and attention dedicated to this manuscript, without hesitation, enriching the quality of the manuscript. The manuscript is revised complying with the reviewers' comments which are addressed one by one. Moreover, any changes in the manuscript have been highlighted within the manuscript in italics blue color in the case of English enriching, otherwise in italics red color. Moreover, in compliance with the reviewer's comment, the text of the manuscript has been completely revised.

C1: There are some new studies on the same topic, in particular liquefaction, that the authors may have missed, which might be beneficial to mention in the introduction for the sake of completeness of the article. These new studies would show the manuscript's relevance to this journal, and hence, the authors are strongly recommended to address any available relevant articles. Below is a list of related articles for enriching the literature review section:
- Inclined Perimeter Drains Performance as Liquefaction Countermeasure Techniques Below Existing Buildings.
- Evaluation of Seismically Induced Soft Sediment Deformation Structures Vis-à-Vis their Probable Earthquake Sources in Kashmir Basin, NW Himalaya.
- Surface Ground Movement Around a Steel Pipe Pile Foundation During Liquefaction Measured by Effective Stress Analysis.
- Numerical Analysis of Shallow Foundations Resting on Granular Columns Embedded in Liquefiable Soil.
- Experimental Investigation on Seismic Compression of Sand Subjected to Multidirectional Cyclic Loads.
- Reliability Analysis of Soil Liquefaction Considering Spatial Variability of Soil Property.
- Experimental Study on Dynamic Modulus and Damping Ratio of Rubber-Sand Mixtures Over a Wide Strain Range.
- Estimation and Application of Strength and Stiffness Reduction Factors of Liquefiable Soil.
- Seismically Evaluate Liquefaction-Induced Steel Tunnel-Sand-Pile Interaction (TSPI) Response.
- Effects of Inclination of Longitudinal and Vertical Acceleration Components of Near-Field Earthquake Records on Seismic Responses of Pile Foundation-Superstructure Systems in Liquefiable Soil Bed.

R1: In response to the reviewer's comments, some new references are addressed in the literature as follows:
"The shear modulus of granular materials is a key parameter dealing with liquefaction and its consequences. There have been several studies focused on this phenomenon in the literature highlighting the role of shear moduli [Chen et al., 2021; Dinesh et al., 2020; Garcıáa-Torres & Madabhushi, 2019; He et al., 2022; Trung et al., 2020; Yousuf & Bukhari, 2020]."
(Pages 1 to 2, Lines: 21 to 25)

Added references:
Chen, Q., Gao, G., Nie, C., Yang, J., Bi, J., & Gu, X. [2021]. "Experimental Investigation on Seismic Compression of Sand Subjected to Multidirectional Cyclic Loads". Journal of Earthquake and Tsunami, 15(05), 2150023. https://doi.org/10.1142/S1793431121500238
Dinesh, N., Banerjee, S., & Rajagopal, K. [2020]. "Numerical Analysis of Shallow Foundations Resting on Granular Columns Embedded in Liquefiable Soil". Journal of Earthquake and Tsunami, 15(03), 2150014. https://doi.org/10.1142/S1793431121500147
Garcıáa-Torres, S., & Madabhushi, G. S. P. [2019]. "Inclined Perimeter Drains Performance as Liquefaction Countermeasure Techniques Below Existing Buildings". Journal of Earthquake and Tsunami, 14(03), 2050015. https://doi.org/10.1142/S1793431120500153
He, H., Li, S., Senetakis, K., Coop, M. R., & Liu, S. [2022]. "Influence of anisotropic stress path and stress history on stiffness of calcareous sands from Western Australia and the Philippines". Journal of Rock Mechanics and Geotechnical Engineering, 14(1), 197–209. https://doi.org/10.1016/j.jrmge.2021.03.015
Trung, N. T., Cuong, D. Q., & Kiyomiya, O. [2020]. "Surface Ground Movement Around a Steel Pipe Pile Foundation During Liquefaction Measured by Effective Stress

	Analysis". Journal of Earthquake and Tsunami, 15(02), 2150010. https://doi.org/10.1142/S179343112150010X Yousuf, M., & Bukhari, K. [2020]. "Evaluation of Seismically Induced Soft Sediment Deformation Structures Vis-à-Vis their Probable Earthquake Sources in Kashmir Basin, NW Himalaya". Journal of Earthquake and Tsunami, 15(01), 2150003. https://doi.org/10.1142/S1793431121500032 C2: Some references need to be written in a unified form. R2: The style of References was changed as per the journal-accepted format. C3: For references over ten years old, you may want to retain only those necessary for your manuscript development. Please delete references older than ten years unless you have discussed them in some detail in the manuscript. R3: In compliance with the reviewer's comment, "Atkinson et al. [1984], Doanh et al., [1997], Da Fonseca " were removed from the reference list.

Evolution of Elastic Shear Modulus During Shearing Under Different Stress Paths Considering Anisotropic Stress History

Fani, Kamran[1], Akhtarpour, Ali[2], Bolouri Bazaz, Jafar[3]

Abstract. Continuous shear wave velocity measurements are conducted on cylindrical triaxial sandy specimens consolidated with isotropic and anisotropic stress histories to characterize the evolution of the elastic shear modulus under different stress paths. The shear wave velocity is measured using an automatic device capable of consecutive measurements of travel time. All specimens were prepared using the Water Sedimentation (WS) method, and after undergoing a stress-controlled path representing the stress history of the specimens, they were subjected to stress-controlled drained shearing along eight different paths. The stress components used in the existing correlations estimating the shear moduli are specified under different stress paths. The results demonstrate that the existing empirical correlations can appropriately be used within the elastic region or the loading surface. However, the accuracy of such models estimating shear moduli might be depreciated as shearing commences, particularly if the stress path involves deviatoric stress, diverging from the expected trends at a specific stress ratio, which is strongly linked to the consolidation stress state. A criterion at which the shear modulus is diverted is also suggested, found to be directly related to the initial stress anisotropy.

1. Introduction

The initial shear modulus of granular material, known as elastic shear modulus, is significantly influenced by both the effective stress state and the void ratio. [Kuwano & Jardine, 2002; Szilvagyi et al., 2016]. The initial or elastic shear modulus (G_0) is associated with the state at which extremely small levels of shear strains (usually less than or about 10^{-6} [-]) are induced in the sample. *The shear modulus of granular materials is a key parameter dealing with liquefaction and its consequences. There have been several studies focused on this phenomenon in the literature highlighting the role of shear moduli*

[1] Ph.D. Candidate, Department of Civil Engineering (CE), Ferdowsi University of Mashhad, Mashhad, Iran. ORCID: https://orcid.org/0000-0002-2557-2254. Email: kamranfani@mail.um.ac.ir.
[2] Associate professor, Department of Civil Engineering (CE), Ferdowsi University of Mashhad, Mashhad, Iran. ORCID: https://orcid.org/0000-0003-1654-0194. Email:akhtarpour@um.ac.ir.
[3] Associate professor, Department of Civil Engineering (CE), Ferdowsi University of Mashhad, Mashhad, Iran. ORCID: https://orcid.org/0000-0002-5106-1845. Email: bolouri@um.ac.ir.

[Chen et al., 2021; Dinesh et al., 2020; Garcıáa-Torres & Madabhushi, 2019; He et al., 2022; Trung et al., 2020; Yousuf & Bukhari, 2020].

So far, extensive experimental investigations have been conducted corroborating the anisotropy in the initial shear modulus of granular materials [Ezaoui & Benedetto, 2009; Fakharian et al., 2019; Kaviani-Hamedani et al., 2021; Kuwano & Jardine, 2002; Szilvagyi et al., 2016]. Some studies on conventional triaxial specimens have also indicated that the shear modulus in each direction is indeed an anisotropic function of both effective stresses, i.e., vertical and horizontal stress components [Dutta et al., 2020; Kuwano & Jardine, 2002; Szilvagyi et al., 2016]. Moreover, the initial shear moduli of granular materials (G_0) are inherently anisotropic due to the microscopic characteristics of the so-called soil fabric [Fakharian et al., 2019; Kaviani-Hamedani et al., 2021; Li et al., 2014; Payan et al., 2016; Teachavorasinskun, 2014; Yu et al., 2013; Zamanian et al., 2021]. However, the role of the soil fabric has been overlooked in the predictive empirical correlations. As a result, existing correlations inevitably predict the same values for two specimens with the same state in terms of effective stress and void ratio but different fabrics [Kaviani-Hamedani et al., 2021; Kuwano & Jardine, 2002; Szilvagyi et al., 2016].

Continuous tracking of the shear modulus was first performed over axial compression stress paths using the triaxial apparatus, capturing variations in shear modulus along the strain-controlled stress paths [Styler & Howie, 2014]. Fakharian et al. and Kaviani-Hamedani et al. [Fakharian et al., 2019; Kaviani-Hamedani et al., 2021] studied the bidirectional shear moduli measurements during the same stress paths, highlighting the depreciation in the accuracy of existing shear modulus correlations due to systematic fabric evolution toward the critical state, resulting in a drop in shear modulus values deviating from expected values. However, [Fakharian et al., 2022] continuously measured the shear moduli over strain-controlled axial compression (AC) and extension (AE) loadings in which different asymptotic values were achieved at fairly large enough axial strain levels (i.e., 18% and 12% of axial strain, respectively), whereas the other possible stress paths were not covered.

In the present research, three series of triaxial experiments considering different stress-controlled, consolidation stress paths, providing corresponding stress histories are intended to examine the existing empirical correlations in the prediction of the vertical shear modulus over such stress paths, hereafter referred to as PSH representing previous stress history. It is worth pointing out that the shear wave velocity in the vertical direction is consecutively measured in all experiments. Subsequently, eight different stress-controlled shearing paths (i.e., L1 to L8 in $q - p'$ stress plane, as shown in Fig.3) are followed towards the critical state line, where $q = \sigma'_v - \sigma'_h$, $p' = (\sigma'_v + 2\sigma'_h)/3$, and σ'_v, σ'_h are the vertical and horizontal effective stress components, respectively. The experiments were conducted under drained conditions throughout all three test series. Following this, the applicability of predictive empirical correlations of shear modulus is scrutinized over shear in different directions. The results reveal dissimilar patterns of shear modulus variations by assigning different shear modes, evidently due to varying ways in which stress components change. Moreover, the results highlight the reasonable accuracy of such correlations within the loading surface (or yield surface), where the element is expected to behave elastically. However, accuracy may diminish beyond this surface, particularly if the stress path involves a systematic increase in deviatoric stress at a specific stress ratio (q/p'), strongly linked with the consolidation stress state.

2. Theoretical Background

A few studies [Hardin, 1978; Hardin & Richart, 1963] introduced a straightforward relationship wherein the initial shear modulus in the vertical direction (i.e., V) is expressed as a function of the mean effective stress (p') and the void ratio function (f_e) expressed as follows:

$$G = C.f_e.p'^n \qquad [1]$$

where "C" and "n" are constant parameters that are inherently related to the soils; f_e is a function of void ratio (e); and $f_e = (2.17 - e)^2/(1 + e)$ as suggested by [Hardin, 1978]. Even Though this function suggests an isotropic state of stress-dependency, Roesler [1979] experimentally demonstrated an anisotropic one in which shear moduli can be determined by two stress components (i.e., vertical and horizontal effective stresses) in the case of the anisotropic and isotropic stress state [Roesler, 1979]. Kuwano and Jardine (2002) suggested that the initial shear modulus of sands under an anisotropic stress state is a function of the void ratio and the effective stress variables $(\sigma'^m_v . \sigma'^n_h)$ as follows:

$$G_{vh} = C_{vh}.f_e.\left(\frac{\sigma'_v}{1\ \mathrm{kPa}}\right)^{m_{vh}}.\left(\frac{\sigma'_h}{1\ \mathrm{kPa}}\right)^{n_{vh}} \qquad [2]$$

where σ'_v and σ'_h stand for the effective vertical and horizontal stresses, respectively. m_{vh}, n_{vh}, and C_{vh} are also constant parameters which are called stress exponents hereafter. The subscripted letters (v and h) stand for the direction and polarization of wave propagation, respectively. [Kaviani-Hamedani et al., 2021] indicated that the stress exponents are not the same, and higher values of stress exponents represent the stronger effective stress component in creating new effective contacts and enhancing the existing contact forces through which the shear wave propagates. Moreover, the values of m_{ij} are not constant and change owing to fabric evolution during shearing, whereas the values of n_{ij} remain constant [Kaviani-Hamedani et al., 2021]. In this study, the values of the stress exponents are expected to be constant during the PSH, as the ratio of σ'_v to σ'_h is not so high that fabric evolution becomes intensive.

3. Testing Equipment and Measuring Devices

The experiments were conducted using a sophisticated automated triaxial apparatus equipped with closed-loop control features (Fig. 1(a)). Shear wave velocity was measured continuously along the vertical direction by dividing the current travel distance by the travel time. The travel distance represents the tip-to-tip distance of the bender element ceramics mounted on both the top platen and pedestal of the triaxial apparatus, as depicted in Fig. 1(b). Since the specimen's height, and thus the travel distance, needed to be adjusted throughout the experiments according to the intended loading path, the current travel distance was determined by taking into account the axial deformations measured by the LVDT. This approach enabled the effortless measurement of the current travel distance, considering both the current specimen height and the constant intrusion length of the bender element ceramics into the specimens. Additionally, the travel time was continuously measured by an automatic module, which is a compact assembly comprising a function generator and oscilloscope (Fig. 1(c)). The function generator was responsible for producing arbitrary transmitting signals with adjustable amplitude, frequency, and burst options. Meanwhile, the oscilloscope facilitated the acquisition of both transmitted and received signals (generated by the function generator and received by the receiver ceramics, respectively)

4. Specimen Preparation and Test Procedure

4.1 Soil Properties

The tested material in this study is a crushed silica sand (i.e., Firuzkuh F161), which is classified as an SP-sand as per USCS (Fig. 2). The gradation analysis demonstrates that it is a fine sand, as presented in Fig. 2a. Moreover, Table 1 encompasses the physical properties of the tested material. The grain-scale SEM (Scanning Electron Microscopy) image of particles suggests that it is susceptible to anisotropic behavior as a subangular sand. It is worth pointing out that this sand is benchmark sand in Iran on which several extensive experimental investigations have been performed [Ahmad & Fakharian, 2020; Fakharian & Kaviani-Hamedani, 2020; Fakharian & Vafaei, 2020; Farahmand et al., 2016b; Kaviani-Hamedani et al., 2023; Shabani & Kaviani-Hamedani, 2023; Vafaei et al., 2021].

4.2 Specimen preparation

Three series of Consolidated Drained (CD) monotonic triaxial tests, each following different PSHs, were conducted on sandy specimens. The specimens had diameters of 71 mm and heights of 160 mm. All specimens were prepared using the "Water Sedimentation" (WS) method as proposed by [Vaid & Chern, 1983]. In this method, a mixture of sand and de-aired water is boiled to remove trapped air bubbles. The mixture is then poured into a mold filled with de-aired water, possibly intensified by gentle tapping to achieve the desired initial density. The upper platen is placed on the soil surface, and after applying 20 kPa of vacuum pressure, the split mold is opened. The accurate height of each specimen is directly measured to determine the current travel distance for the tests.

4.3 Test Program

The test program in this study consists of three series of drained triaxial experiments as detailed in Table 2, encompassing parameters such as relative density, confining stress, and stress ratio ($\eta = q/p'$). The relative density of each specimen corresponds to the end of consolidation, determined using the back-analysis method proposed by [Verdugo et al., 1996] calculated by weighing the specimen after the tests. In Fig. 3, the consolidation stress paths entail a complex drained stress-controlled trajectory toward the maximum mean effective pressure ($p' = 400$ kPa), meeting the desiredη (i.e., 1 to 2 path) and then is unloaded by 200 kPa while maintaining η unchanged (2 to 3 path). As depicted in Figs. 3(a) and 3(b), three η values were employed in this study (η=0 representing an idealized isotropic initial stress state, and η=0.4 and -0.4 corresponding to anisotropic stress states, respectively). The consolidation stress path establishes the initial stress state or initial stress anisotropy, hereafter referred to as Previous Stress History (PSH), with point 3 marking the end of PSH. Additionally, for $\eta = 0$, two stepped stress paths were utilized, with either vertical or horizontal effective stresses kept constant to determine the stress exponents m and n, as elucidated in Eq. [2]. This method was employed by [Kaviani-Hamedani et al., 2021]. Furthermore, the stress exponents were determined through multi-variable regression analysis, as discussed in subsequent sections.

In the next step, the experiments were followed with drained stress-controlled shearing stress paths (L1 to L8) towards the critical state line, as illustrated in Figs. 3(c) to 3(e). The critical state lines of Firuzkuh sand for axial compression and extension (i.e., $CSL_C \approx 1.4$ and $CSL_E \approx -1$) are also presented for further clarification, as reported by [Farahmand et al., 2016a] and [Fakharian et al., 2022]. It is noteworthy that the shear wave velocity measurement is conducted all over the PSH and shearing stress path, tracking the variations of shear modulus.

4.4 Signal Interpretation

Interpreting the signals from the bender element test is widely acknowledged as a challenging task, prompting numerous experimental and fundamental investigations [Camacho-Tauta et al., 2015; Lee & Santamarina, 2005; Rahman et al., 2016; Viggiani & Atkinson, 1995]. Fig. 4 depicts the methodology employed to determine the time of travel. As depicted in Fig. 4, five received waves are illustrated at various strain levels, while the transmitted signal remains constant throughout. These waves exhibit iterative translocations with each measurement, yet their general waveform remains relatively consistent, as previously noted by Kaviani-Hamedani et al. 2021. The travel time required to transmit mechanical shear waves from one bender element to the other is calculated using the first major peak method. In this method, the travel time is defined as the difference between the peak points of the transmitted wave and the first major peak points of the received waves.

5. Test Results

5.1 Shear modulus over the PSH

Several empirical correlations have been proposed to address the initial shear modulus under both isotropic and anisotropic stress states, as represented by Eq. [1]. The stress exponents (m_{vh} and n_{vh} for the vertical and horizontal stress components, respectively) describe the stress dependency of the shear modulus to the associated stress components. Notably, these stress exponents are not necessarily identical due to soil anisotropy, resulting in discrepancies in the stress dependency of the shear modulus. This phenomenon has also been observed in previous studies [Kuwano & Jardine, 2002; Pennington et al., 1997].

The stress exponents and the coefficient of Eq. [2] can be determined (e.g., m_{vh}, n_{vh}, C_{vh}) through non-linear multivariable regression as presented in Figs. 5(a) to 5(d) as insets. The non-linear multivariable regression was conducted on a natural logarithmic transformation taken from both sides of Eq. [2], which yields

$$\ln(G_{vh}/fe) = \ln(C_{vh}) + m_{vh}\ln\left(\frac{\sigma'_v}{1\ \mathrm{kPa}}\right) + n_{vh}.\ln\left(\frac{\sigma'_h}{1\ \mathrm{kPa}}\right) \qquad [3]$$

Fig. 5 encompasses the normalized shear modulus by void ratio function against stress state i.e., $\left(\frac{\sigma'_v}{1\ \mathrm{kPa}}\right)^{m_{vh}}.\left(\frac{\sigma'_h}{1\ \mathrm{kPa}}\right)^{n_{vh}}$, considering the figured-out stress exponents on the associated data set. In Fig. 5(a), the data points for η=0 are plotted against the corresponding stress state along with the fitted line. The results indicate that the empirical equation used for predicting shear modulus can reasonably approximate the data (i.e., 70% of data points within a 10% error margin). The stress exponents for the horizontal and vertical stress components are found to be 0.13 and 0.33, respectively, highlighting the anisotropic stress dependency of shear modulus. In Fig. 5(b), void ratio variations over the PSH stage for two specimens which are supposed to be sheared under L1 and L2 stress paths are displayed. It can be observed that the specimens undergo densification as the stress path progresses from point 1 to point

2, followed by a slight expansion in soil structure during the unloading stress path from 2 to 3. As shown in Fig. 5(c), the values of m_{vh} and n_{vh} for η=0.4 are 0.25 and 0.30, respectively, resulting in an underestimated predictive equation. However, there is a strong correlation observed for η=-0.4 along the Previous Stress History (PSH) stress paths, with an accuracy ratio of over 96% as shown in Fig. 5(e). In Figs. 5(d) and 5(f), the variations in void ratio for two typical specimens are depicted in which a similar volume change pattern can be observed. Furthermore, as depicted in Fis. 5(g), applying $m_{vh} = 0.20$ and $n_{vh} = 0.32$ allows the correlation to predict 70% of all shear modulus values regardless of η, while maintaining a 10% error margin.

Thus, the application of such an empirical equation appears to be a reasonable method for predicting shear modulus. Nonetheless, it is essential to recognize that the Previous Stress History (PSH) paths did not expose the specimens to high-stress ratio levels, thereby minimizing the potential for deviation from expected values.

5.2 Shear modulus over the shear

Fig. 6 depicts the stress-strain response of specimens consolidated under η=0, where eight different stress paths (L1 to L8) were initiated, starting from an isotropic stress state along various directions. The variations in void ratios, commencing from relatively similar values, are also depicted in Fig. 6(b). The graph emphasizes the anisotropic nature of the volume change response. The magnified views of deviatoric stress and volumetric strain over axial strain are shown in Figs. 6(c) and 6(d), respectively.

It is imperative to acknowledge most experiments cannot reach the well-defined critical state due to the fashion managed for the application of stress path (stress-controlled) resulting in exceedance of axial strain and specimen failure, particularly in the case of specimens with post-softening regimes or those with isotropic changes in stress levels.

As anticipated, stress paths L3 and L7 only marginally mobilized trivial deviatoric stress values due to isotropic variations along the shear paths. However, deviatoric stress increases rapidly, especially for L1 and L5, where it is expected to increase and decrease, respectively. Furthermore, the mobilized shear strength along the L1 stress path is more pronounced compared to L5, attributed to soil anisotropy, as frequently observed in other studies comparing AC and AE loading modes, where the contractive regime is more pronounced in extension loading. This observation is clearly illustrated in Fig. 6(d), highlighting the more contractive responses in stress paths toward the extension critical state line (L4) compared to those moving toward the compressional critical state line (e.g., L8). This trend was also observed in other specimens under anisotropic initial stress states (i.e., η=0.4 and η=-0.4), as frequently noted in previous studies [Fakharian et al., 2022; Fakharian & Kaviani-Hamedani, 2020; Kato et al., 2001; Keyhani & Haeri, 2013; Rodriguez & Lade, 2013; Sivathayalan & Vaid, 2002].

Fig. 7 illustrates the variations in shear modulus over the shear paths L1 to L8, consolidated under different η values. Generally, the shear moduli exhibit variation from the end of the Previous Stress History (PSH) state (i.e., point 3) and are strongly influenced by the stress state, resulting in an increase in shear moduli with the growth in the stress state. However, a linear relationship is not observed during the PSH, particularly for L1 and L5 stress paths regardless of η values, where their trends deviate from linear expectations (e.g., L1, L2, L5 for η=0). Nonetheless, the expected linear trend observed during the PSH state can also be observed (e.g., L3 and L7 stress paths for η=0), as these shear paths occur after the PSH stress paths without any pronounced deviation. This observation further supports the reported deviation from the empirical correlation previously noted by [Fakharian et al., 2019; Kaviani-Hamedani et al., 2021; Kuwano & Jardine, 2002].

Subsequently, the normalized trends of shear moduli for all stress paths with η=0 are presented in Fig. 8 for further elucidation. In Fig. 8(a), the variation of shear modulus over the Previous Stress History (PSH) and shear stages is depicted. Here, the data points during the PSH form an approximately linear trend between two dashed lines, while the onset of the L1 shear stress path initially aligns with the fitted trend and then deviates (marked as the state point), as illustrated in the magnified inset. In Fig. 8(b), although the shear modulus initially conforms more closely to expectations compared to L1, a similar deviation point from the trend is observed in the L2 stress path, denoted by the star symbol. Fig. 8(c) illustrates a similar pattern for L3 stress paths, where the mean effective stress decreases isotropically. This result indicates that the trend of shear modulus can be accurately predicted by the empirical equation and decreases as the shear stress path aligns with the fitted lines. Hence, the deviation point cannot be assumed for any stress path; it may either be postponed, accelerated, or even avoided depending on the intended stress path. In Fig. 8(d), a pattern similar to the L2 stress path is observed in the L4 path, while a more pronounced deviation point occurs in the L5 stress path. Additionally, similar trends are observed for the other paths (i.e., L6, L7, and L8 presented in parts (f), (g), and (h), respectively), as previously described. Therefore, despite the overall trend being influenced by the stress paths and associated variations in stress states, deviations from the values expected by empirical equations may occur.

Kuwano and Jardin (2002), Dutta et al. (2020), and Kaviani-Hamedani et al. (2021) held the intense changes in the soil fabric responsible for the diversion points in sandy soils [Dutta et al., 2020; Kaviani-Hamedani et al., 2021; Kuwano & Jardine, 2002]. However, some recent contributions used these points as a criterion to define the yield surface of cohesive soils, separating the elastic and plastic zones [Jung et al., 2007; Kantesaria & Sachan, 2022]. There are several methods available to experimentally determine yield points, each selecting a specific point from a curve that describes a macroscopic measure against deformations. Wood (1990) proposed a method utilizing the deviatoric stress-strain curve, which necessitates the direct and accurate measurement of radial deformation under drained conditions.

It is important to note that Wood's suggestion was based on the earlier works of Tatsuoka (1972) and Tatsuoka and Ishihara (1974), who emphasized the preference for undisturbed samples of sandy soils to preserve the in-situ soil fabric. Unfortunately, acquiring undisturbed samples proved to be insufficient for conducting distinct tests. Consequently, the adopted method allowed for the determination of the entire yield surface from a single undisturbed specimen. Consequently, other methods commonly used for clayey soils could theoretically be applied to sands as well.

Another challenge encountered was intentional variations in mean effective stress (p'), which occurred as per the intended shear stress path. This variation in p' values compromised the desired constant values necessary to generate εv-p' curves for each experiment. Therefore, the application of $\varepsilon_v - \varepsilon_a$ and $q - \varepsilon_a$ were preferred instead as a common criterion and a method was required to determine the yield surface which might come up with some slight discrepancies as compared with the established method's findings. Each of these criteria may become irrelevant for some stress paths (e.g., $q-\varepsilon_a$ for L3 and L7 stress paths) as compared with $\varepsilon_v-\varepsilon_a$.

On the other hand, in the context of bounding surface models, it is postulated that stress states consistently reside within an imaginary surface known as the loading surface. Furthermore, this surface is assumed to exhibit purely elastic behavior, adhering to Hooke's law, where stress is directly proportional to strain within this region. To explain this matter for the experiments on sandy soil, the elastic zone (or the loading surface theoretically defined and used in the constitutive models), which is expected to be small in granular materials (as clearly described by [Dafalias, 1981; Taiebat & Dafalias, 2008] in bounding surface models) is specified as presented in Fig. 9. As expected, the pure elastic part of stress-strain response of sandy specimens is significantly small comparing with the cohesive soils. To find the location of the yield surface, separating the elastic and plastic zone in $q-p'$ stress plane, these points are overlaid on the intended stress paths in Fig. 10 shaping oval regions in red color.

As shown in Fig. 10(a), the loading surfaces are too small and considerably affected by the initial stress anisotropy by which the specimens were consolidated as reported by [Dafalias, 1981; Taiebat & Dafalias, 2008]. The observed diversion points are also overlaid on the stress plane by the star symbol in these figures. In Fig. 10(a), the diversion points can be observed over the L1, L2, L8, L4, L5, and L6 stress paths at certain stress ratios on the $q-p'$ stress state (one positive and one negative), shaping loci hereafter is called the diversion line. The slope of diversion lines are 0.3 and -0.423 for η=0, whereas these ratios for η=0.4 and -0.4 are 0.68 & 0.04 and 0.05 and -0.577 =, respectively. Therefore, the results highlight the facts that the empirical equations can effortlessly be applicable within the elastic zone (or loading surface) and even beyond that in the case that the stress path does not pass the diversion lines. The loading surface is not a good criterion to identify the diversion points at least for the tested material; rather the diversion points occur at the diversion lines which are also considerably affected by the initial stress anisotropy as shown in Fig. 10(d). In Fig. 10(d), the zones in which the shear modulus is not diverted from the predicted line are presented by two lines representing the stress ratios of η_C and η_E. The subscripted 'C' and 'E' stand for compressional and extensional loading. The graph corroborates that this zone and associated stress ratios (i.e., η_C and η_E) rotates with a consolidation stress ratio like the yield surface. Fig. 10(e) clearly illustrates the no-diversion zones against the consolidation stress ratio. As the consolidation stress ratio increases, η_C and η_E ratios increase as well. It seems the diversion lines highlight the stress ratios at which the fabric evolution is intensified. Therefore, the existing empirical correlations are expected to work more accurately within these zones which are significantly affected by the initial stress anisotropy. Still, it should be considered that increasing deviatoric stress paths depreciate prediction accuracy.

6. Predictive Empirical Model

To predict the shear modulus under different stress anisotropy, including the PSH and shearing in all stress paths, a predictive model is suggested using the multivariable regression method. Such predictive empirical models can be effective in estimating the normalized shear modulus (G/f_e). So far, several predictive empirical models have been developed using multivariable regression, which generally is expressed as the product of the stress state as shown in Eq. [2]. In this study, the proposed formulation, predicting the normalized shear modulus can be expressed as the following formulas:

$$\frac{G}{f_e} = c.(p')^m.(1+\eta)^n \qquad [4]$$

where m and n are exponents which are assumed to be constant over all the stress paths. η is the current stress ratio (i.e., q/p'), considering the stress anisotropy all over the experiment. The constants of this formulation (i.e., m, n, and c) were figured out by employing non-linear multivariable regression.

Please note that while the proposed empirical equation deals with the initial (or elastic) shear modulus under different stress states, measured at various strain levels, it should not be interpreted as a shear modulus at different strain levels. Furthermore, despite the equation put forth by Golchin and Lashkari (2014), this formulation neglects energy conservation in a closed-loop path.

The non-linear multivariable regression was conducted on a natural logarithmic transformation taken from both sides of Eq. [4], which yields

$$\ln(G/f_e) = \ln(c) + m.\ln(p') + n.\ln(1+\eta) \qquad [5]$$

Fig. 11 illuminates the results of the predictive empirical model for all stress paths, including the PSH stage and shearing stress paths. As can be seen, the model predictions are in quite good agreement with the captured values over all experiments, highlighting the capability of the suggested expression along different stress paths. Even though the findings of this study corroborated that the existing form of the applicability of existing empirical models depreciates when the fabric evolution becomes intense. Regarding this matter, Fig. 12 demonstrates the error in predicting the shear modulus over the shearing stress paths. Fig. 12(a) presents bubble graphs over the stress paths of shearing along different directions (i.e., L1 to L8) for specimens consolidated isotropically, in which the error at each stress state is visually illustrated with the given bubble size and color. The results indicate that the error generally evolves from negligible values at the isotropic stress state (around 1% to 6%) and becomes significant as the stress paths move towards the compression and extension critical state lines. It can be seen that the primary changes in error values are observed in the vicinity of the critical state lines whereas these are much less than near the isotropic stress state (i.e., $q = 0$). Following this, Fig. 12(b) shows the error map by which the regions on $q - p'$ stress plane with a certain error level value are drawn and hatched. The graph clearly demonstrates that the proposed empirical equation can effectively predict the shear modulus in a wide range of stress states with error levels less than 10% and small regions representing higher levels of error (i.e., 10% to 15% and >15%) remain. Therefore, even though the fabric-evolution-induced diversion of shear modulus (shown in Fig. 8) can depreciate the precision of empirical models, reasonable predictions can be expected across a wide range of stress states, excluding the proximity of the critical state lines at which the influences of fabric evolution on shear modulus expected to be more pronounced. Figs.12(c) to 12(f) similarly present the error level changes over the shearing paths for anisotropically consolidated specimens with $\eta = 0.4$ and -0.4. The graphs illuminate the same pattern of changes in error levels so that they increase by approaching the critical state lines. However, the shape of the region across which the error level<10% is deformed. The border of this shape can be determined by the distances from the end of the PSH stage (as a reference point) to the vertices, and the longer the distance is, the greater scope for changing the stress state along the vertex is. Therefore, this region inevitably deforms to have a shorter thickness whenever the reference stress state is near the critical state line since the fabric evolution and subsequent increase in prediction error is expected to occur sooner. Another interesting point is that the isotropic stress path (e.g., L7 as shown in Fig. 12(b)) cannot depreciate the accuracy of prediction for isotropically consolidated specimens. However, the error levels in prediction become pronounced along L7 stress paths for $\eta = -0.4$ and 0.4, due to differences in fabric evolution during the consolidation stage and an isotropic stress path can evolve changes in soil fabric differently.

7. Conclusion

The current paper focuses on scrutinizing the existing empirical correlations to predict the initial shear modulus under the isotropic and anisotropic initial stress states. Besides, the shear modulus variations are tracked over the different shear paths. All the experiments were conducted on a subangular sandy soil employing the triaxial apparatus with continuous bender element tests all over the experiment. The most important findings can be stated as follows:

1. The existing empirical equations are applicable over the isotropic and anisotropic stress state as long as the fabric changes do not become intense so that the predicted values might be diverted from the lines fitted through the data points measured prior to any intense fabric evolution.
2. The diversion lines (i.e., η_{Com} and η_{Ex}) frame the zone (so-called no-diversion zones) in which no diversion from the predicted shear modulus is expected.
3. The existing correlations can effortlessly work within these zones which enclose the loading surface. The diversion from the predicted values is more pronounced over the stress paths that involve an intense growth/drop in deviatoric stress (e.g., L1 or L5 in the case of $\eta = 0$). Diversions from expected values were not found distinct for the loading paths during which the changes in the stress ratio over the shear were not so different from the consolidation stress ratios (e.g., L3 and L7).

4. Diversion lines can be significantly affected by the initial stress anisotropy previously experienced. The No-diversion zones rotate with the consolidation stress ratio like the yield surface.
5. The stress ratio of diversion lines (η_{Com} and η_{Ex}) increases with growth in the consolidation stress ratio.

Acknowledgment

The authors would like to acknowledge the contributions of Global Material Testing Manufacturers (Global M.T.M.) for their sincere support and cooperation in equipment setup and accessories development to enable the testing program of this study. Special thanks are due to Farid Shabani for his technical support during the different stages of developing the required accessories.

References

Ahmad, A., & Fakharian, K. [2020]. *Effect of Stress Rotation and Intermediate Stress Ratio on Monotonic Behavior of Granulated Rubber – Sand Mixtures*. *32*(4), 1–11. https://doi.org/https://doi.org/10.1061/(ASCE)MT.1943-5533.0003054

Camacho-Tauta, J. F., Cascante, G., Da Fonseca, A. V., & Santos, J. A. [2015]. "Time and frequency domain evaluation of bender element systems". *Geotechnique*, *65*(7), 548–562. https://doi.org/10.1680/geot.13.P.206

Chen, Q., Gao, G., Nie, C., Yang, J., Bi, J., & Gu, X. [2021]. "Experimental Investigation on Seismic Compression of Sand Subjected to Multidirectional Cyclic Loads". *Journal of Earthquake and Tsunami*, *15*(05), 2150023. https://doi.org/10.1142/S1793431121500238

Dafalias, Y. F. [1981]. "The Concept and Application of the Bounding Surface in Plasticity Theory". *Physical Non-Linearities in Structural Analysis, 1*, 56–63. https://doi.org/10.1007/978-3-642-81582-9_9

Dinesh, N., Banerjee, S., & Rajagopal, K. [2020]. "Numerical Analysis of Shallow Foundations Resting on Granular Columns Embedded in Liquefiable Soil". *Journal of Earthquake and Tsunami*, *15*(03), 2150014. https://doi.org/10.1142/S1793431121500147

Dutta, T. T., Otsubo, M., Kuwano, R., & O'Sullivan, C. [2020]. "Evolution of shear wave velocity during triaxial compression". *Soils and Foundations*.

Ezaoui, A., & Benedetto, H. Di. [2009]. "Experimental measurements of the global anisotropic elastic behaviour of dry Hostun sand during triaxial tests, and effect of sample preparation". *Géotechnique*, *59*(7), 621–635.

Fakharian, K., Hamedani, F. K., Parandian, I., & Aghdam, M. J. [2019]. "Investigation of fabric evolution using bidirectional shear wave velocity measurements". *7th International Symposium on Deformation Characteristics of Geomaterials (IS-Glasgow 2019)*, *92*, 3008. https://doi.org/10.1051/e3sconf/20199203008

Fakharian, K., & Kaviani-Hamedani, F. [2020]. "Influence of Initial Anisotropy, Stress Path and Principal Stress Rotation on Monotonic Behavior of Clean and Mixed Sands". *Key Engineering Materials*, *857*, 417–430. https://doi.org/10.4028/www.scientific.net/kem.857.417

Fakharian, K., Kaviani-Hamedani, F., & Imam, S. M. R. [2022]. "Influences of initial anisotropy and principal stress rotation on the undrained monotonic behavior of a loose silica sand". *Canadian Geotechnical Journal*, *59*(6), 847–862. https://doi.org/10.1139/cgj-2020-0791

Fakharian, K., & Vafaei, N. [2020]. "Effect of Density on Skin Friction Response of Piles Embedded in Sand by Simple Shear Interface Tests". *Canadian Geotechnical Journal*, *ja*.

Farahmand, K., Lashkari, A., & Ghalandarzadeh, A. [2016a]. "Firoozkuh sand: introduction of a benchmark for geomechanical studies". *Iranian Journal of Science and Technology, Transactions of Civil Engineering*, *40*(2), 133–148. https://doi.org/10.1007/s40996-016-0009-0

Farahmand, K., Lashkari, A., & Ghalandarzadeh, A. [2016b]. "Firoozkuh Sand: Introduction of a Benchmark for Geomechanical Studies". *Iranian Journal of Science and Technology - Transactions of Civil Engineering*, *40*(2), 133–148. https://doi.org/10.1007/s40996-016-0009-0

Garcıáa-Torres, S., & Madabhushi, G. S. P. [2019]. "Inclined Perimeter Drains Performance as Liquefaction Countermeasure Techniques Below Existing Buildings". *Journal of Earthquake and Tsunami*, *14*(03), 2050015. https://doi.org/10.1142/S1793431120500153

Hardin, B. O. [1978]. "The nature of stress-strain behavior for soils". *From Volume I of Earthquake Engineering and Soil Dynamics--Proceedings of the ASCE Geotechnical Engineering Division Specialty Conference,* *June 19-21, 1978, Pasadena, California. Sponsored by Geotechnical Engineering Division of ASCE in Cooperation With:, Proceeding*.

Hardin, & Richart. [1963]. "Elastic wave velocities in granular soils". *Journal of the Soil Mechanics and Foundations Division, ASCE 89, No. SM1*, 33–65.

He, H., Li, S., Senetakis, K., Coop, M. R., & Liu, S. [2022]. "Influence of anisotropic stress path and stress history on stiffness of calcareous sands from Western Australia and the Philippines". *Journal of Rock Mechanics and Geotechnical Engineering*, *14*(1), 197–209. https://doi.org/10.1016/j.jrmge.2021.03.015

Jung, Y.-H., Cho, W., & Finno, R. J. [2007]. "Defining yield from bender element measurements in triaxial stress probe experiments". *Journal of Geotechnical and Geoenvironmental Engineering*, *133*(7), 841–849.

Kantesaria, N., & Sachan, A. [2022]. "Small-strain shear modulus and yielding characteristics of compacted high-plasticity clay". *Géotechnique*, *72*(5), 424–437. https://doi.org/10.1680/jgeot.20.P.089

Kato, S., Ishihara, K., Towhata, I., AKIRA SATO, M. Z. H., Kato, S., Ishihara, K., & Towhata, I. [2001]. "Undrained shear characteristics of saturated sand under anisotropic consolidation". *Soils and Foundations*, *41*(1), 1–11. http://www.mendeley.com/research/geology-volcanic-history-eruptive-style-yakedake-volcano-group-central-japan/

Kaviani-Hamedani, F., Esmailzade, M., Adineh, K., Shafiei, M., & Shirkavand, D. [2023]. "Quantifying three‐dimensional sphericity indices of irregular fine particles from 2D images through sequential sieving tests". *Granular Matter*, *26*(4). https://doi.org/https://doi.org/10.1007/s10035-023-01376-1 ORIGINAL REPORT 2

Kaviani-Hamedani, F., Fakharian, K., & Lashkari, A. [2021]. "Bidirectional Shear Wave Velocity Measurements to Track Fabric Anisotropy Evolution of a Crushed Silica Sand during Shearing". *International Journal of Geoenvironmental and Geotechnical Engineering*. https://doi.org/doi.org/10.1061/(ASCE)GT.1943-5606.0002622

Keyhani, R., & Haeri, S. M. [2013]. *Evaluation of the e ect of anisotropic consolidation and principle stress rotation on undrained behavior of silty sands*. *20*, 1637–1653.

Kuwano, R., & Jardine, R. J. [2002]. "On the applicability of cross-anisotropic elasticity to granular materials at very small strains". *Géotechnique*, *52*(10), 727–749. https://doi.org/10.1680/geot.2002.52.10.727

Lee, J.-S., & Santamarina, J. C. [2005]. "Bender elements: performance and signal interpretation". *Journal of Geotechnical and Geoenvironmental Engineering*, *131*(9), 1063–1070. https://doi.org/10.1061/(ASCE)1090-0241(2005)131:9(1063)

Li, B., Zeng, X., & Ming, H. [2014]. "Experimental method to study the effects of fabric anisotropy on elastic shear modulus of sand". *Geotechnical Testing Journal*, *37*(4). https://doi.org/10.1520/GTJ20120118

Payan, M., Khoshghalb, A., Senetakis, K., & Khalili, N. [2016]. "Effect of particle shape and validity of Gmax models for sand: A critical review and a new expression". *Computers and Geotechnics*, *72*, 28–41. https://doi.org/10.1016/j.compgeo.2015.11.003

Pennington, D. S., Nash, D. F. T. T., & Lings, M. L. [1997]. "Anisotropy of G0 shear stiffness in Gault Clay". *Geotechnique*, *47*(3), 391–398. https://doi.org/10.1680/geot.1997.47.3.391

Rahman, M. E., Pakrashi, V., Banerjee, S., & Orr, T. [2016]. "Suitable waves for bender element tests: Interpretations, errors and modelling aspects". *Periodica Polytechnica Civil Engineering*, *60*(2), 145–158. https://doi.org/10.3311/PPci.7952

Rodriguez, N. M., & Lade, P. V. [2013]. "Effects of principal stress directions and mean normal stress on failure criterion for cross-anisotropic sand". *Journal of Engineering Mechanics*, *139*(11), 1592–1601. https://doi.org/10.1061/(ASCE)EM.1943-7889.0000595

Roesler, S. K. [1979]. "Anisotropic shear modulus due to stress anisotropy". *Journal of the Geotechnical Engineering Division*, *105*(7), 871–880. https://doi.org/10.1016/0148-9062(79)90065-2

Shabani, F., & Kaviani-Hamedani, F. [2023]. "Cyclic response of sandy subsoil layer under traffic-induced principal stress rotations: Application of bidirectional simple shear apparatus". *Soil Dynamics and Earthquake Engineering*. https://doi.org/10.1016/j.soildyn.2022.107573

Sivathayalan, S., & Vaid, Y. P. [2002]. "Influence of generalized initial state and principal stress rotation on the undrained response of sands". *Canadian Geotechnical Journal*, *39*(1), 63–76.

Styler, M. A., & Howie, J. A. [2014]. "Continuous monitoring of bender element shear wave velocities during triaxial testing". *Geotechnical Testing Journal*, *37*(2), 218–229. https://doi.org/10.1520/GTJ20120098

Szilvagyi, Z., Hudacsek, P., & Ray, R. P. [2016]. "Soil shear modulus from resonant column, torsional shear and bender element tests". *International Journal of Geomate 10:(2)*, 1822–1827.

https://doi.org/10.21660/2016.20.39871

Taiebat, M., & Dafalias, Y. F. [2008]. "SANISAND: Simple anisotropic sand plasticity model". *International Journal for Numerical and Analytical Methods in Geomechanics*, *32*(8), 915–948. https://doi.org/10.1002/nag.651

Teachavorasinskun, S. [2014]. "Combined Inherent and Stress Induced Anisotropy on the Initial Shear Modulus of Sand". *Electronic Journal of Geotechnical Engineering*, *19*, 8861–8869. https://doi.org/10.1155/2020/7841824

Trung, N. T., Cuong, D. Q., & Kiyomiya, O. [2020]. "Surface Ground Movement Around a Steel Pipe Pile Foundation During Liquefaction Measured by Effective Stress Analysis". *Journal of Earthquake and Tsunami*, *15*(02), 2150010. https://doi.org/10.1142/S179343112150010X

Vafaei, N., Fakharian, K., & Sadrekarimi, A. [2021]. "Sand-sand and sand-steel interface grain-scale behavior under shearing". *Transportation Geotechnics*, *30*, 100636. https://doi.org/https://doi.org/10.1016/j.trgeo.2021.100636

Vaid, Y. P., & Chern, J.-C. [1983]. "Effect of static shear on resistance to liquefaction". *Soils and Foundations*, *23*(1), 47–60. https://doi.org/10.3208/sandf1972.23.47

Verdugo, R., Ishihara, K., & Verdugo. [1996]. "The steady state of sandy soils". *Soils and Foundations*, *36*(2), 81–91. https://doi.org/10.3208/sandf.36.2_81

Viggiani, G., & Atkinson, J. H. [1995]. "Interpretation of bender element tests". *Geotechnique*, *45*(1), 149–154. https://doi.org/10.1680/geot.1995.45.1.149

Yousuf, M., & Bukhari, K. [2020]. "Evaluation of Seismically Induced Soft Sediment Deformation Structures Vis-à-Vis their Probable Earthquake Sources in Kashmir Basin, NW Himalaya". *Journal of Earthquake and Tsunami*, *15*(01), 2150003. https://doi.org/10.1142/S1793431121500032

Yu, H., Zeng, X., Li, B., & Ming, H. [2013]. "Effect of fabric anisotropy on liquefaction of sand". *Journal of Geotechnical and Geoenvironmental Engineering*, *139*(5), 765–774.

Zamanian, M., Payan, M., Jafarzadeh, F., Ranjbar, N., & Senetakis, K. [2021]. "Evolution of Dynamic Properties of Cross-Anisotropic Sand Subjected to Stress Anisotropy". *Journal of Geotechnical and Geoenvironmental Engineering*, *147*(7). https://doi.org/10.1061/(asce)gt.1943-5606.0002541

Table 1. Physical properties of Firuzkuh sand No. 161

Property	Value
C_c	0.88
C_u	1.9
D_{50} (mm)	0.22
G_s	2.65
e_{max}	0.931
e_{min}	0.56

Table 2. Outline of the testing program

Test number	η	Void ratio	D_r (%)	Shear stress path
1	0	0.814	31.6	L1
2	0	0.816	30.9	L2
3	0	0.811	32.3	L3
4	0	0.821	29.6	L4
5	0	0.843	27.0	L5
6	0	0.826	28.3	L6
7	0	0.817	30.7	L7
8	0	0.814	31.5	L8
9	0.4	0.827	28.0	L1
10	0.4	0.809	32.9	L2
11	0.4	0.811	32.3	L3
12	0.4	0.816	31.0	L4
13	0.4	0.806	33.7	L5
14	0.4	0.824	28.8	L6
15	0.4	0.830	27.2	L7
16	0.4	0.818	30.4	L8
17	-0.4	0.798	35.8	L1
18	-0.4	0.815	31.2	L2
19	-0.4	0.819	30.2	L3
20	-0.4	0.816	31.0	L4
21	-0.4	0.831	27.0	L5
22	-0.4	0.809	32.9	L6
23	-0.4	0.816	31.1	L7
24	-0.4	0.814	31.5	L8

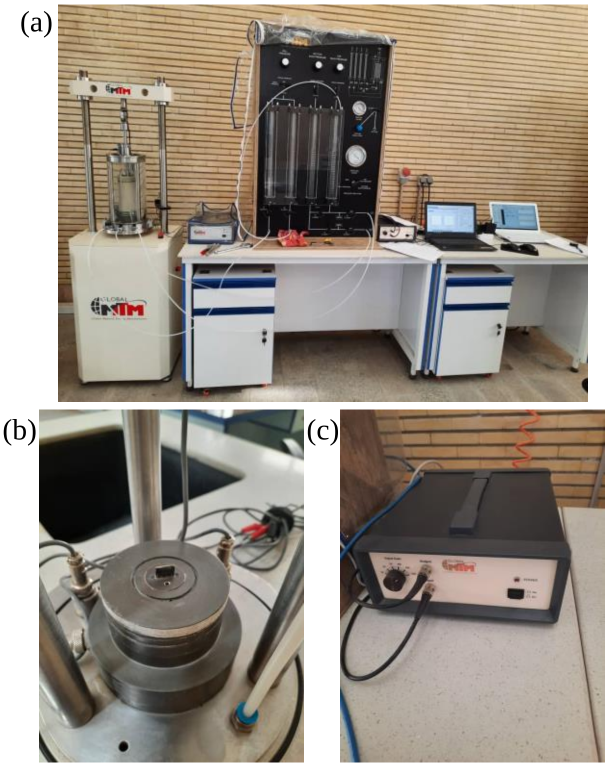

Fig. 1 Testing device: (a) Triaxial apparatus; (b) bender piezoelectric mounted on the pedestal; (c) automatic small-strain device (manufactured by Global MTM)

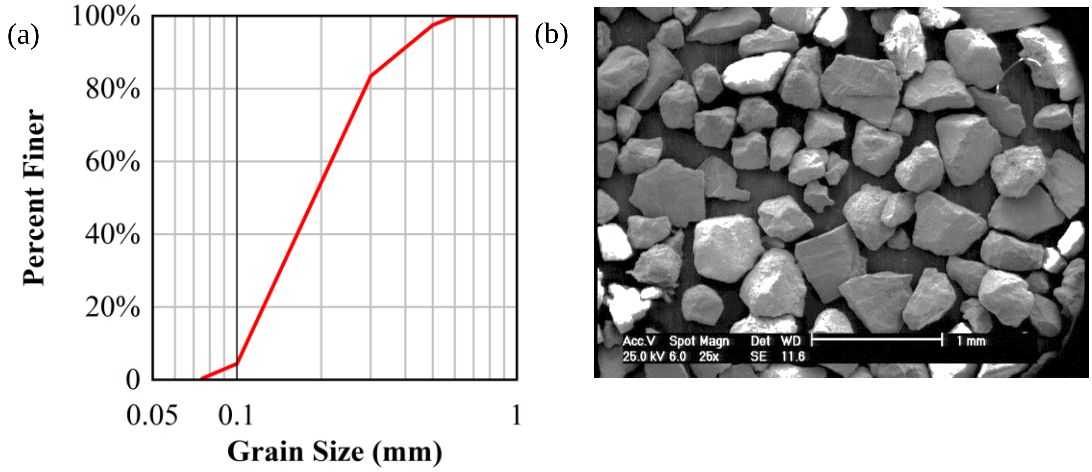

Fig. 2 Firuzkuh sand: (a) Grading analysis; (b) SEM image presenting the grain shape

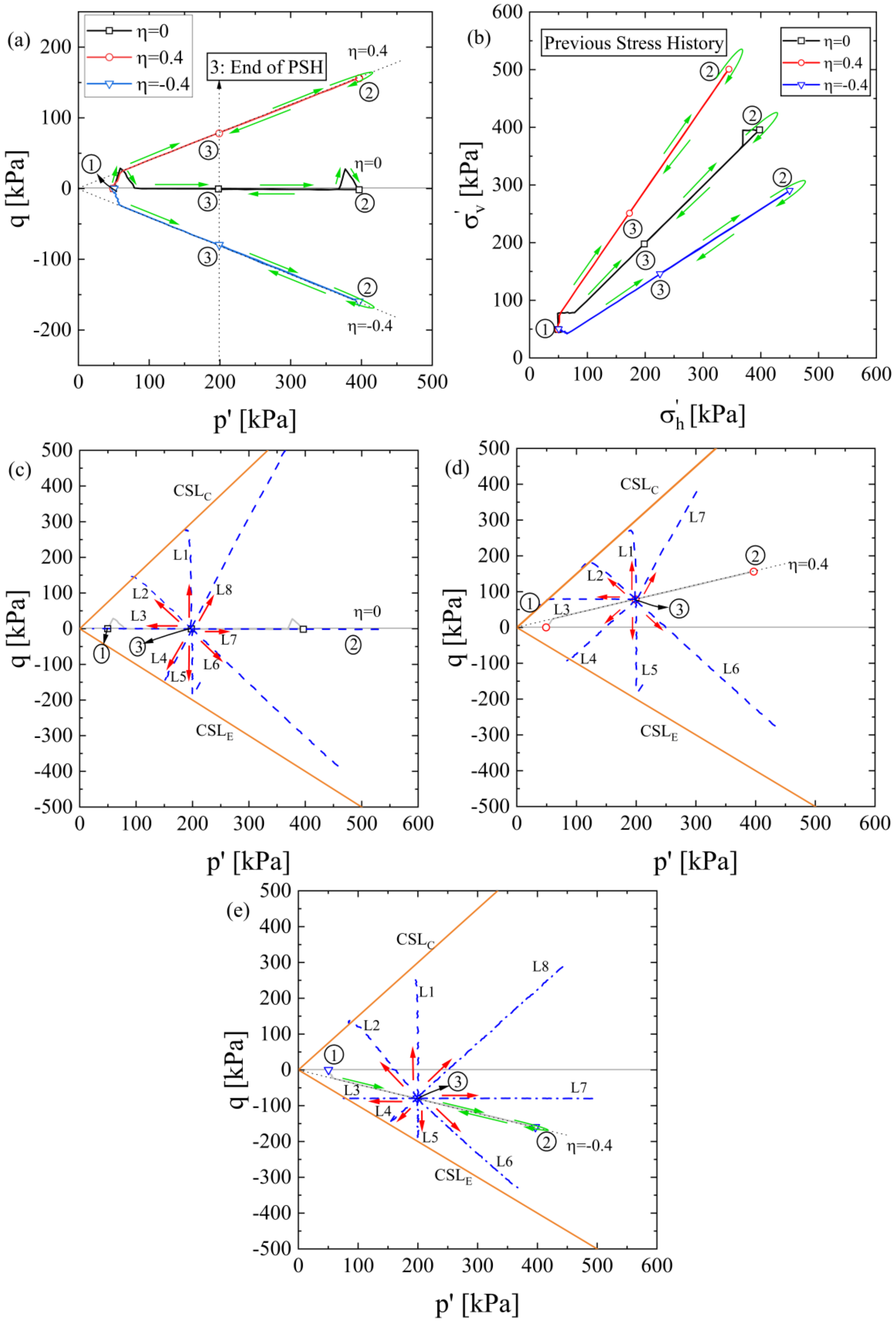

Fig. 3 The PSH and shearing stress path: (a) PSH in $q-p'$stress plane; (b) PSH in $\sigma_v'-\sigma_h'$ plane; (c) Shearing stress path ($\eta=0$); (d) Shearing stress path ($\eta=0.4$); (e) Shearing stress path ($\eta=-0.4$)

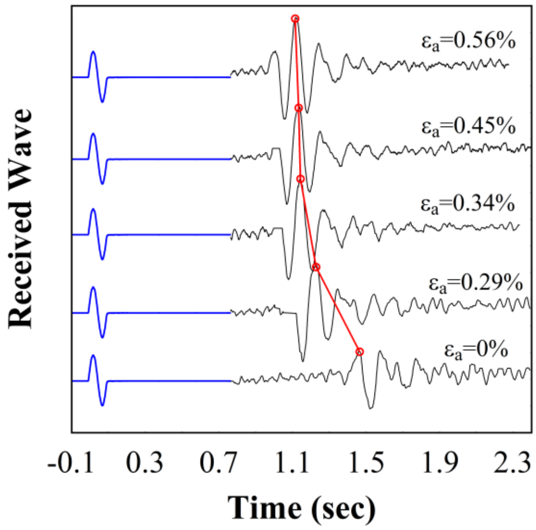

Fig. 4 First major peak signal interpretation of bender element tests over the experiment

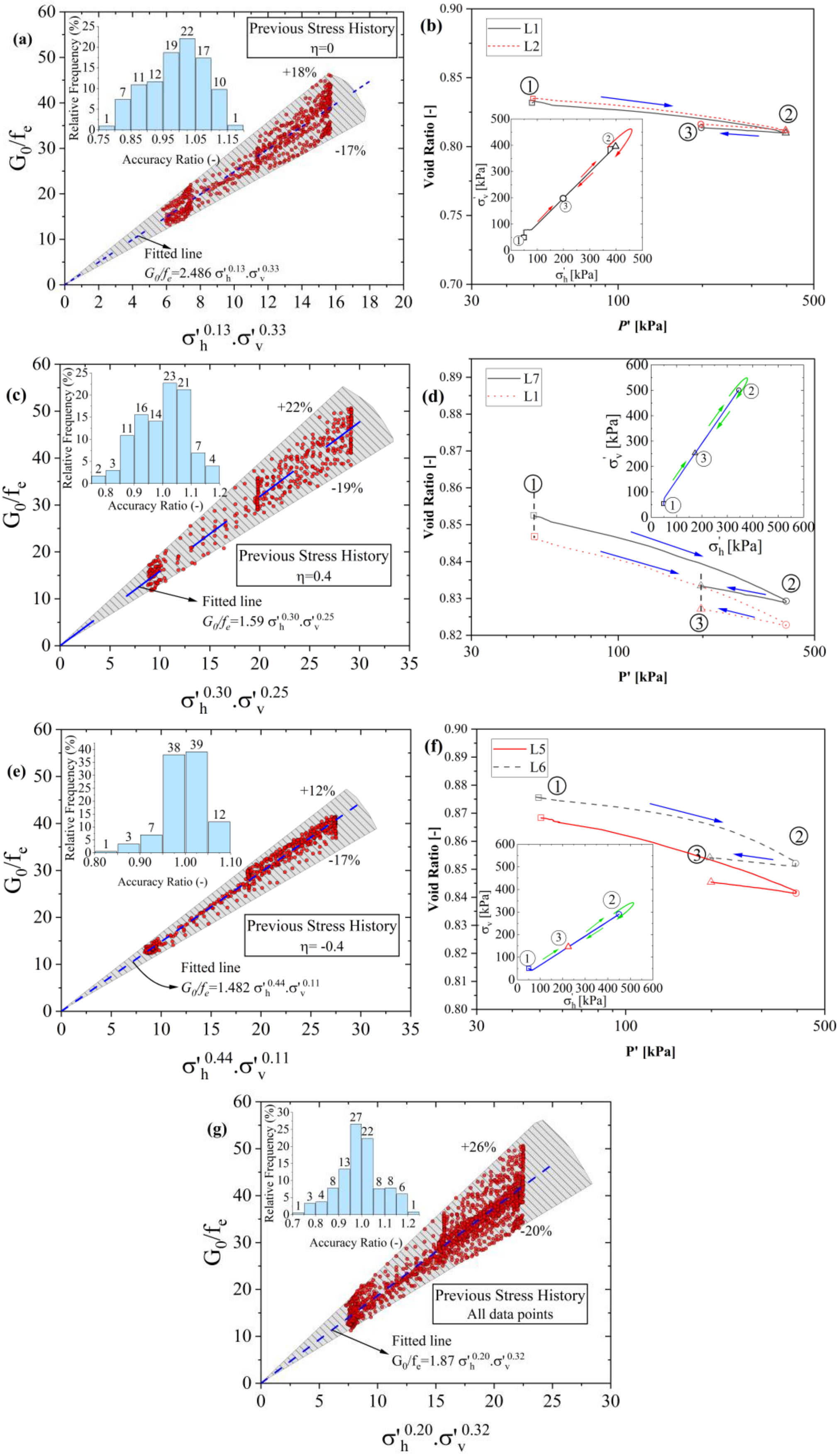

Fig. 5 Determination of stress exponents over the PSH paths and void ratio changes: (a) & (b) η=0; (c) & (d) η=0.4; (e) & (f) η=-0.4; (g) all stress ratios

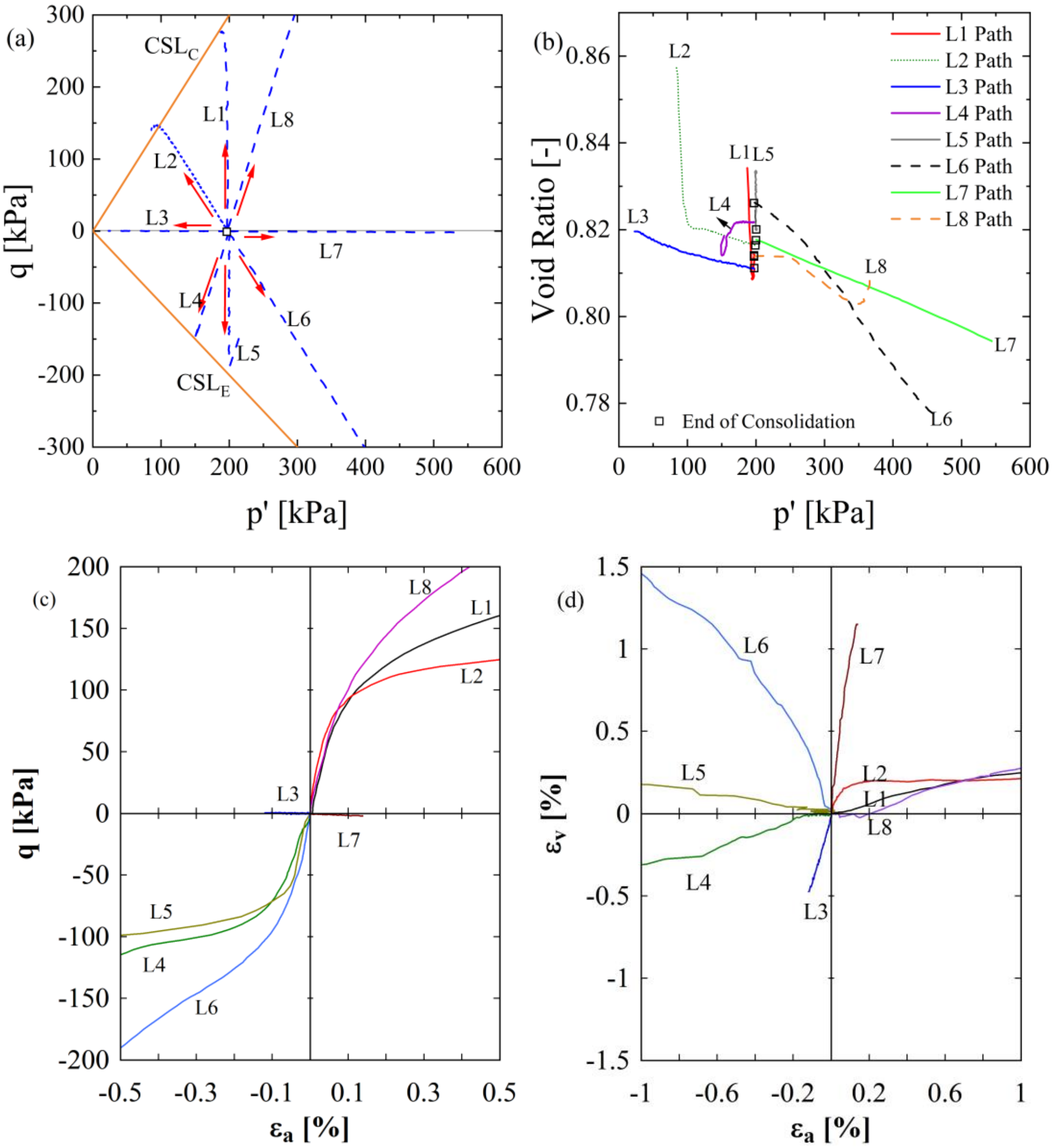

Fig. 6 The stress-strain response of L1 to L8 under $\eta = 0$: (a) stress paths in $q - p'$ stress plane; (b) void ratio changes versus p'; (c) $q - \varepsilon_a$; (d) $\varepsilon_v - \varepsilon_a$

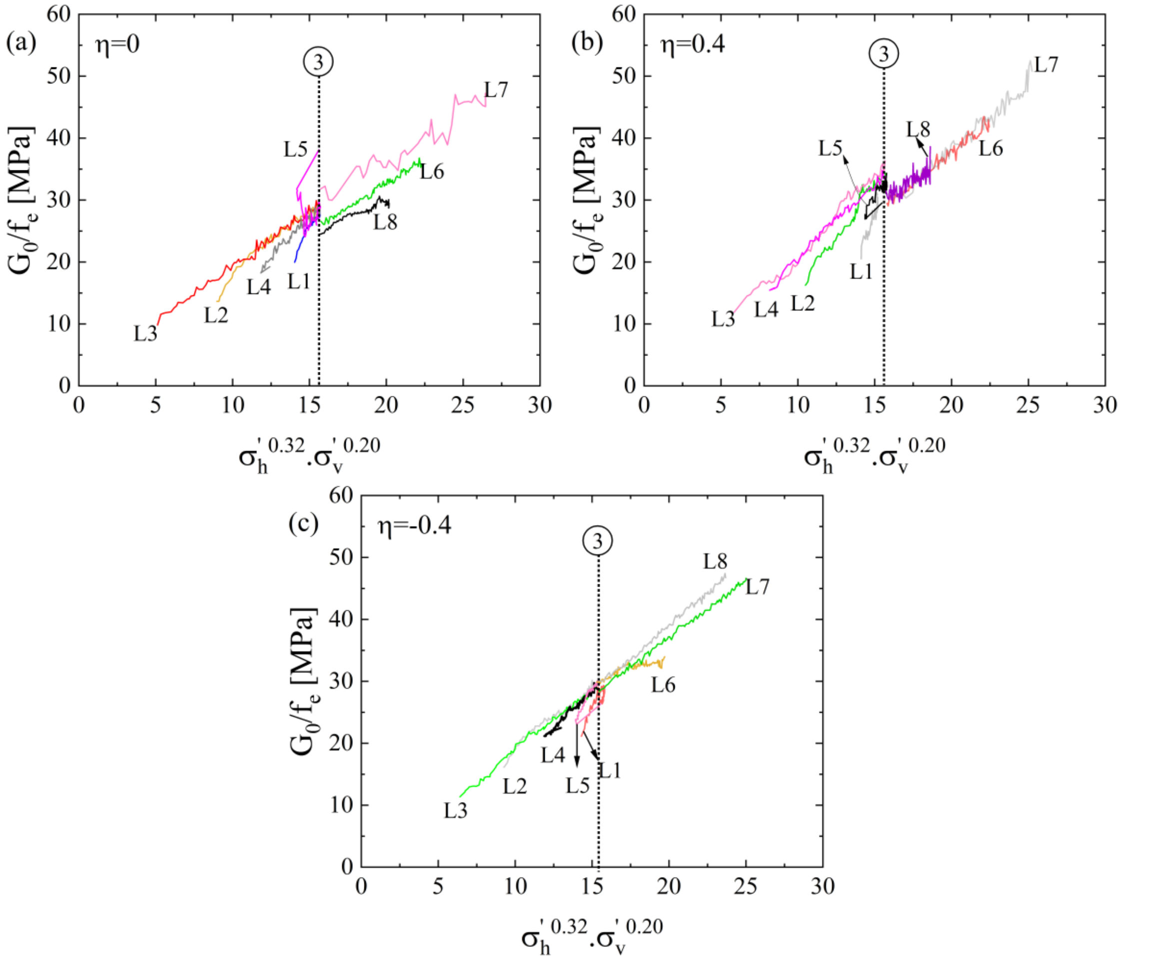

Fig. 7 Variation of shear modulus during shear paths under different initial stress state: (a) η=0; (b) η=0.4; (c) η=-0.4

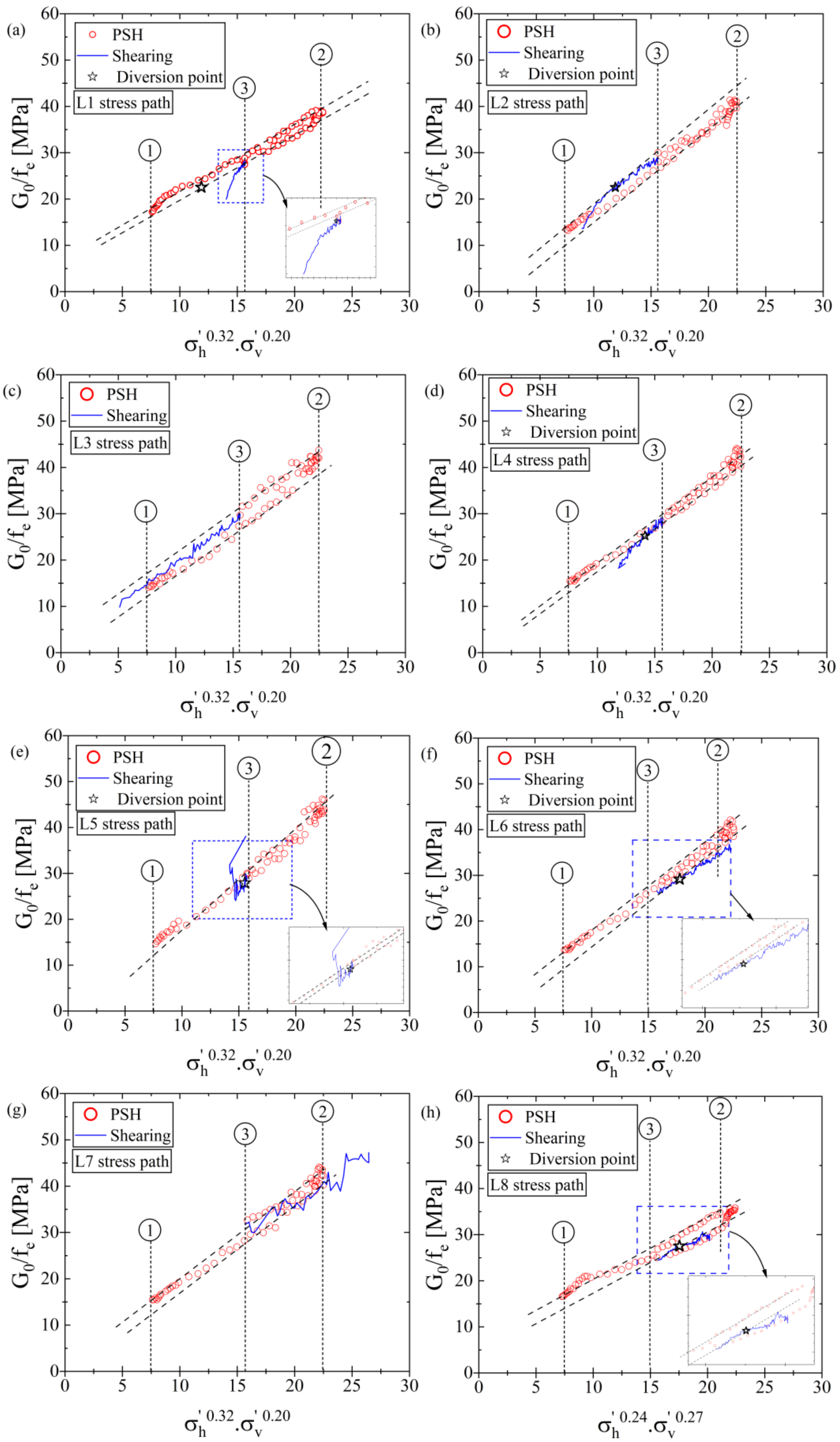

Fig. 8 Shear modulus variations over the shear paths and diversion points for: (a) L1; (b) L2; (c) L3; (d) L5; (e) L6; (f) L7; (g) L7; (h) L8

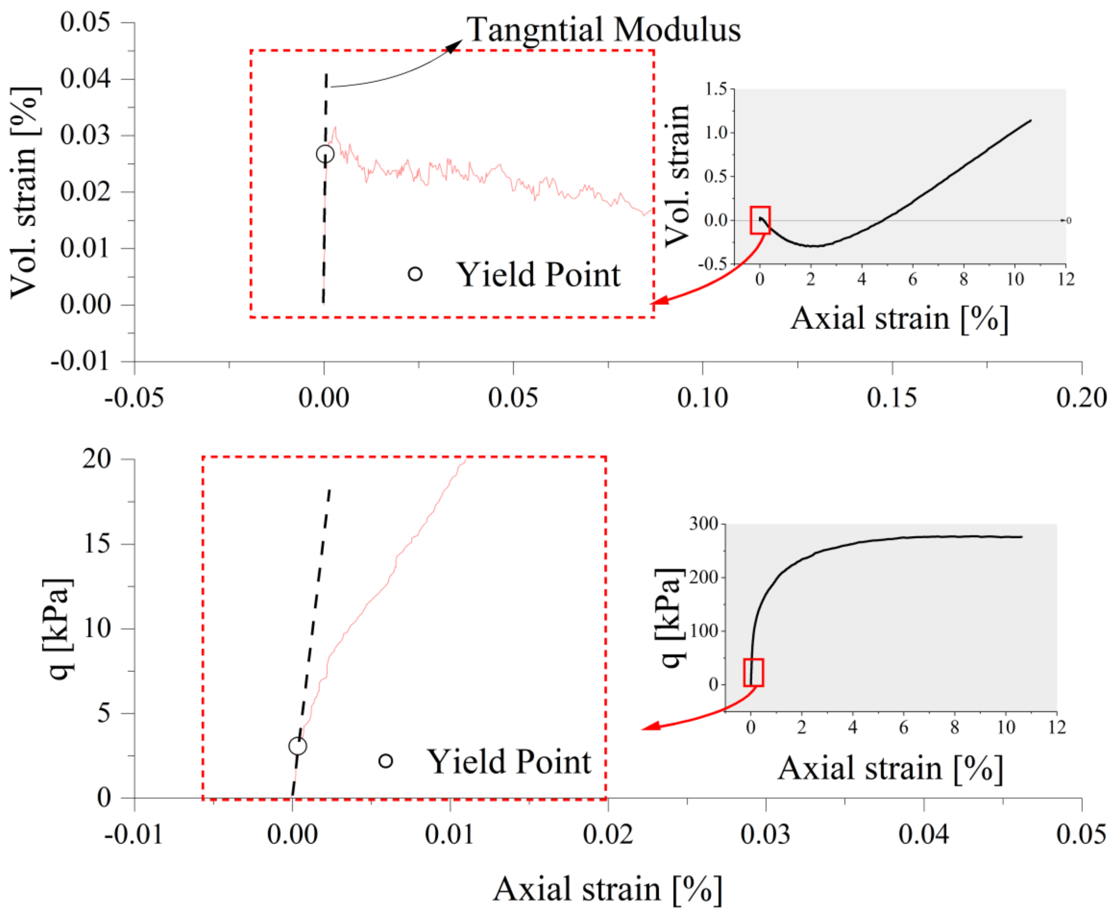

Fig. 9 Yield point detection criterion (Experiment L1 under η = 0)

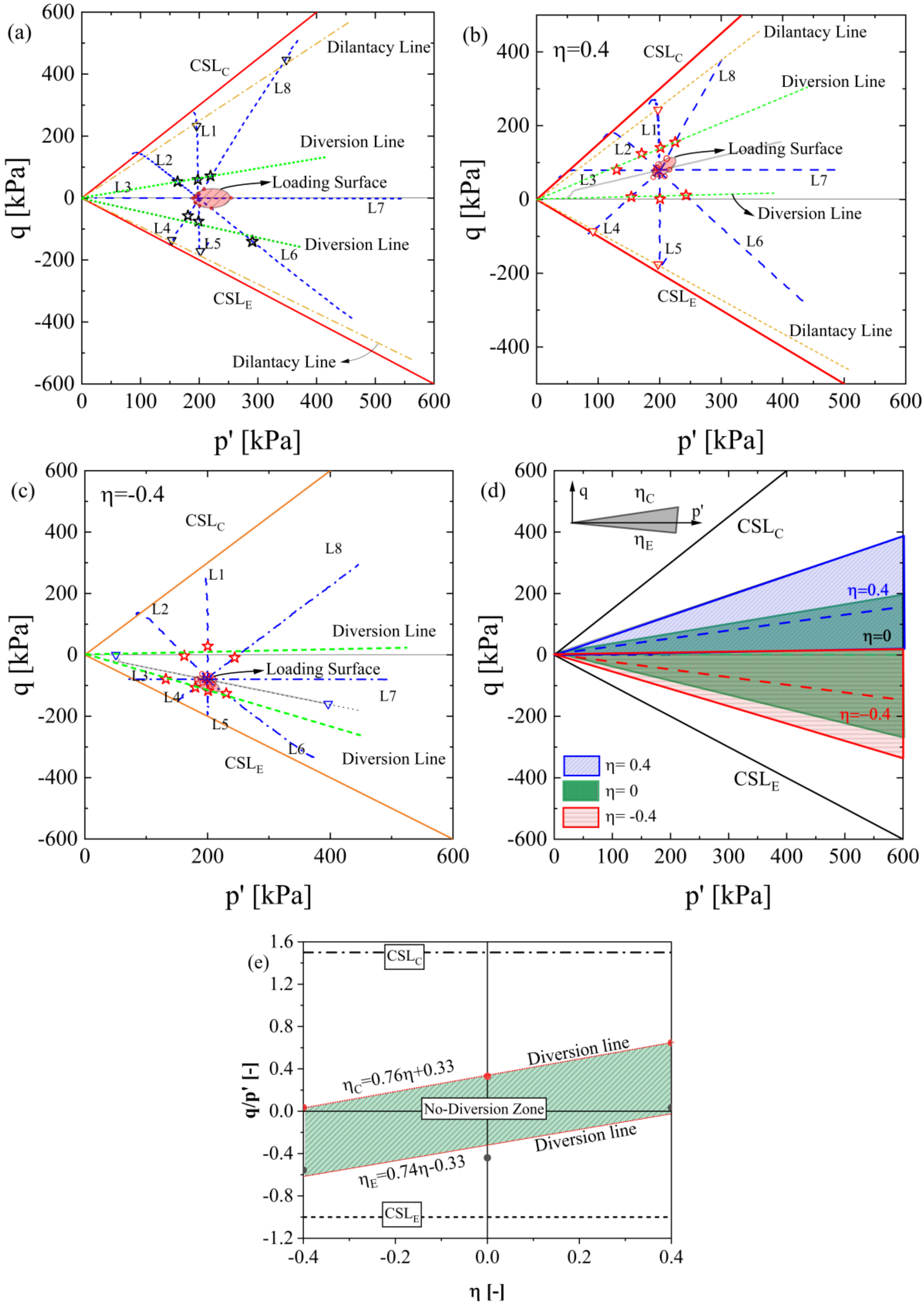

Fig. 10 Diversion Lines and loading surface for specimens with: (a) $\eta = 0$; (b) $\eta = 0.4$; (c) $\eta = -0.4$; (d) No-diversion zones in $q - p'$ stress plane; (e) No-diversion zone vs η

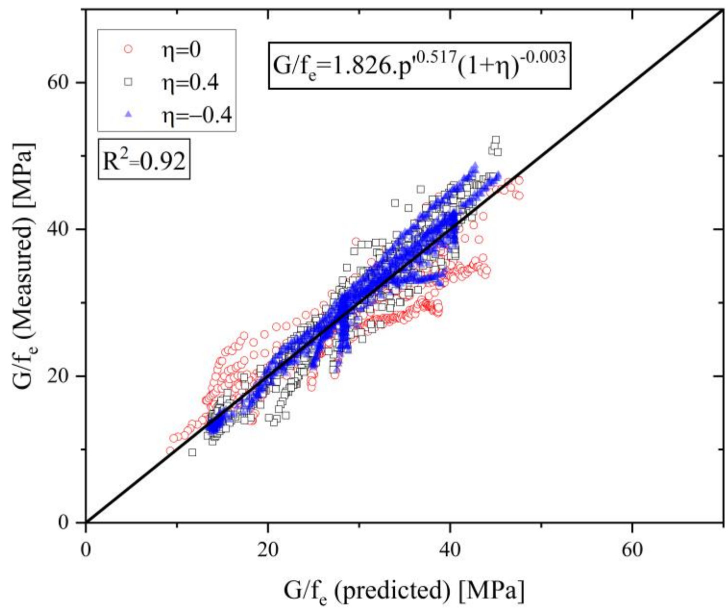

Fig. 11 Comparison between the measured and predicted values of normalized shear modulus over all experiments

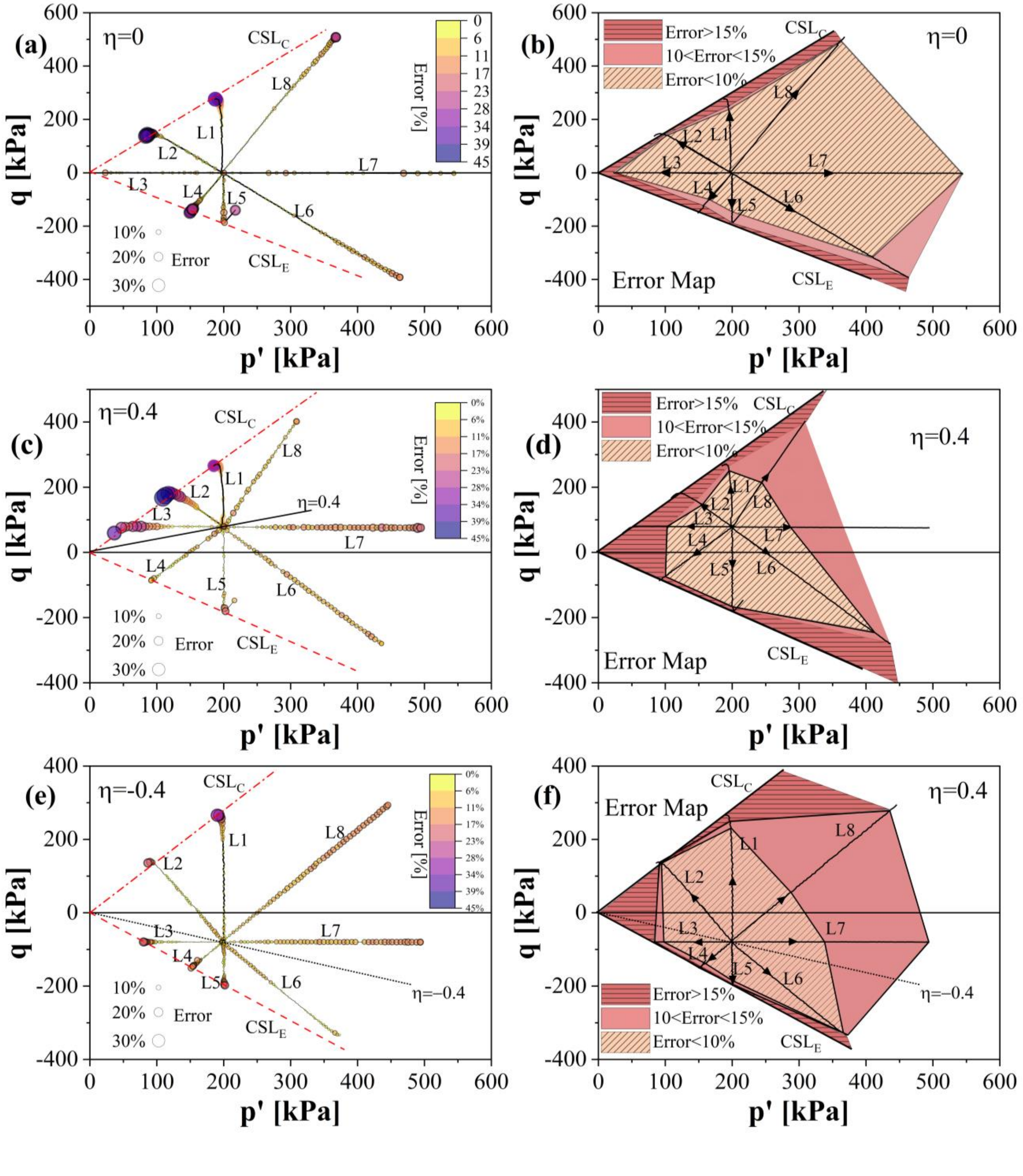

Fig. 12 Error level changes and map for: (a) and (b): $\eta = 0$; (c) and (d): $\eta = 0.4$; (e) and (f): $\eta = -0.4$

Reviewer #1:
C0: Reviewer #1: The manuscript may be accepted for publication as is. **R0:** Thanks indeed for the time and attention dedicated to this manuscript, without hesitation, enriching the quality of the manuscript.
Reviewer #2:
Co: The revised manuscript has been significantly improved. However, my main concern goes to the manuscript's subject, which falls outside the main keywords of the journal. Instead, it is more suitable for a specialized geotechnical engineering journal. To somehow resolve this issue, the authors are recommended to consider the following comments: **R0:** Thanks indeed for the time and attention dedicated to this manuscript, without hesitation, enriching the quality of the manuscript. The manuscript is revised complying with the reviewers' comments which are addressed one by one. Moreover, any changes in the manuscript have been highlighted within the manuscript in *italics blue color* in the case of English enriching, otherwise in italics *red color*. Moreover, in compliance with the reviewer's comment, the text of the manuscript has been completely revised.
C1: There are some new studies on the same topic, in particular liquefaction, that the authors may have missed, which might be beneficial to mention in the introduction for the sake of completeness of the article. These new studies would show the manuscript's relevance to this journal, and hence, the authors are strongly recommended to address any available relevant articles. Below is a list of related articles for enriching the literature review section: - Inclined Perimeter Drains Performance as Liquefaction Countermeasure Techniques Below Existing Buildings. - Evaluation of Seismically Induced Soft Sediment Deformation Structures Vis-à-Vis their Probable Earthquake Sources in Kashmir Basin, NW Himalaya. - Surface Ground Movement Around a Steel Pipe Pile Foundation During Liquefaction Measured by Effective Stress Analysis. - Numerical Analysis of Shallow Foundations Resting on Granular Columns Embedded in Liquefiable Soil. - Experimental Investigation on Seismic Compression of Sand Subjected to Multidirectional Cyclic Loads. - Reliability Analysis of Soil Liquefaction Considering Spatial Variability of Soil Property. - Experimental Study on Dynamic Modulus and Damping Ratio of Rubber-Sand Mixtures Over a Wide Strain Range. - Estimation and Application of Strength and Stiffness Reduction Factors of Liquefiable Soil. - Seismically Evaluate Liquefaction-Induced Steel Tunnel-Sand-Pile Interaction (TSPI) Response. - Effects of Inclination of Longitudinal and Vertical Acceleration Components of Near-Field Earthquake Records on Seismic Responses of Pile Foundation-Superstructure Systems in Liquefiable Soil Bed. **R1:** In response to the reviewer's comments, some new references are addressed in the literature as follows: *"The shear modulus of granular materials is a key parameter dealing with liquefaction and its consequences. There have been several studies focused on this phenomenon in the literature highlighting the role of shear moduli* [Chen et al., 2021; Dinesh et al., 2020; Garcıáa-Torres & Madabhushi, 2019; He et al., 2022; Trung et al., 2020; Yousuf & Bukhari, 2020]*."* ***(Pages 1 to 2, Lines: 21 to 25)***

Added references:

Chen, Q., Gao, G., Nie, C., Yang, J., Bi, J., & Gu, X. [2021]. "Experimental Investigation on Seismic Compression of Sand Subjected to Multidirectional Cyclic Loads". *Journal of Earthquake and Tsunami*, *15*(05), 2150023. https://doi.org/10.1142/S1793431121500238

Dinesh, N., Banerjee, S., & Rajagopal, K. [2020]. "Numerical Analysis of Shallow Foundations Resting on Granular Columns Embedded in Liquefiable Soil". *Journal of Earthquake and Tsunami*, *15*(03), 2150014. https://doi.org/10.1142/S1793431121500147

Garcıáa-Torres, S., & Madabhushi, G. S. P. [2019]. "Inclined Perimeter Drains Performance as Liquefaction Countermeasure Techniques Below Existing Buildings". *Journal of Earthquake and Tsunami*, *14*(03), 2050015. https://doi.org/10.1142/S1793431120500153

He, H., Li, S., Senetakis, K., Coop, M. R., & Liu, S. [2022]. "Influence of anisotropic stress path and stress history on stiffness of calcareous sands from Western Australia and the Philippines". *Journal of Rock Mechanics and Geotechnical Engineering*, *14*(1), 197–209. https://doi.org/10.1016/j.jrmge.2021.03.015

Trung, N. T., Cuong, D. Q., & Kiyomiya, O. [2020]. "Surface Ground Movement Around a Steel Pipe Pile Foundation During Liquefaction Measured by Effective Stress Analysis". *Journal of Earthquake and Tsunami*, *15*(02), 2150010. https://doi.org/10.1142/S179343112150010X

Yousuf, M., & Bukhari, K. [2020]. "Evaluation of Seismically Induced Soft Sediment Deformation Structures Vis-à-Vis their Probable Earthquake Sources in Kashmir Basin, NW Himalaya". *Journal of Earthquake and Tsunami*, *15*(01), 2150003. https://doi.org/10.1142/S1793431121500032

C2: Some references need to be written in a unified form.

R2: The style of References was changed as per the journal-accepted format.

C3: For references over ten years old, you may want to retain only those necessary for your manuscript development. Please delete references older than ten years unless you have discussed them in some detail in the manuscript.

R3: In compliance with the reviewer's comment, "Atkinson et al. [1984], *Doanh et al., [1997], Da Fonseca* " were removed from the reference list.